Available online at www.sciencedirect.com

ScienceDirect

Geochimica et Cosmochimica Acta 288 (2020) 248–261

Geochimica et Cosmochimica Acta

www.elsevier.com/locate/gca

Methane thermometry in deep-sea hydrothermal systems: Evidence for re-ordering of doubly-substituted isotopologues during fluid cooling

J. Labidi [a,b,*], E.D. Young [a], T. Giunta [c,d], I.E. Kohl [a,e], J. Seewald [f], H. Tang [a], M.D. Lilley [g], G.L. Früh-Green [h]

[a] Department of Earth, Planetary, and Space Sciences, UCLA, Los Angeles, CA, USA
[b] Université de Paris, Institut de physique du globe de Paris, CNRS, Paris, France
[c] IFREMER, Unité des Géosciences Marines, 29280 Plouzané, France
[d] Université de Bretagne Occidentale, Laboratoire Géosciences Océan, 29280 Plouzané, France
[e] Thermo Fisher Scientific, Bremen, Germany
[f] Marine Chemistry and Geochemistry Department, Woods Hole Oceanographic Institution, Woods Hole, MA, USA
[g] School of Oceanography, University of Washington, Seattle, USA
[h] Department of Earth Sciences, Eidgenössische Technische Hochschule Zurich (ETH-Z), Zurich, Switzerland

Received 1 April 2020; accepted in revised form 11 August 2020; Available online 20 August 2020

Abstract

Deep-sea hydrothermal fluids are often enriched in carbon dioxide, methane, and hydrogen. Methane effuses from metal-rich black smokers such as the Rainbow hydrothermal field, at temperatures higher than 200 °C. At the Lost City field, CH_4 emanates from alkaline fluids at <100 °C. The abundance of the rare, mass-18 CH_4 isotopologues, $^{13}CH_3D$ and $^{12}CH_2D_2$, can mitigate degeneracies in the conventional isotopic signatures of methane. We studied the isotopologue compositions of methane from the Rainbow, Lucky Strike, Von Damm, and Lost City hydrothermal fields. At Rainbow, where the vented fluids are at ~360 °C, our coupled $\Delta^{12}CH_2D_2$ - $\Delta^{13}CH_3D$ data establish that methane is in internal equilibrium at 343^{+41}_{-35} °C. This may track the formation temperature of abiotic methane, or it may be the result of equilibration of methane isotopologues within the carrier fluid. Lucky Strike and Von Damm have fluid temperatures <300 °C and although $\Delta^{13}CH_3D$ values are indistinguishable from those at Rainbow, $^{12}CH_2D_2$ abundances are marginally higher. At Lost City, $\Delta^{13}CH_3D$ data show a range of values, which at face value correspond to apparent temperatures of between 265^{+28}_{-24} °C and 158^{+16}_{-14} °C, far hotter than fluid temperatures. A unique aspect of the Lost City data is the range of large $^{12}CH_2D_2$ excesses. The $\Delta^{12}CH_2D_2$ data correspond to temperatures of between 101^{+9}_{-8} °C and 69^{+4}_{-4} °C, showing a near-perfect match with fluid temperatures. We find that mixing scenarios involving microbial methane may not account for all of the isotope data. We suggest that $\Delta^{12}CH_2D_2$ values, unlike $\Delta^{13}CH_3D$ values, are prone to near-complete re-equilibration at host fluid temperatures. We suggest that $^{13}CH_3D$ isotopologue data are consistent with abiotic methane being synthesized at ~350 °C. On the other hand, $^{12}CH_2D_2$ isotopologue ordering records post formation residence temperatures. We explore a possible mechanism decoupling the re-equilibration systematics of the doubly-substituted isotopologues.

Keywords: Abiotic methane; Doubly-substituted isotopologues; High-resolution mass spectrometry; Hydrothermalism; Black smokers

* Corresponding author at: Université de Paris, Institut de Physique du globe de Paris, CNRS, Paris, France.
E-mail address: labidi@ipgp.fr (J. Labidi).

https://doi.org/10.1016/j.gca.2020.08.013
0016-7037/

1. INTRODUCTION

Deep-sea hydrothermal fluids host mantle-derived CO_2 and various forms of reduced carbon that include methane, C_{2+} alkanes, formate, and a variety of unsaturated molecules (Charlou et al., 2000, 2002, 2010; Holm and Charlou, 2001; Konn et al., 2009; Lang et al., 2010; McDermott et al., 2015; Reeves et al., 2014; Welhan, 1988; Welhan and Craig, 1979). So-called 'black smokers' vent hydrothermal fluid with exit temperatures >300 °C and show significant amounts of molecular hydrogen (Fig. 1), which may allow for the abiotic reduction of CO and/or CO_2 to methane (Berndt et al., 1996; Horita and Berndt, 1999; Jones et al., 2010; McCollom, 2013, 2016; McCollom et al., 2010; McCollom and Seewald, 2001; Neubeck et al., 2011; Okland et al., 2014; Oze et al., 2012; Seewald et al., 2006). In the laboratory, abiotic methane formation is sluggish (McCollom and Seewald, 2007) but may be enhanced by the presence of a catalyst, typically a Fe-Ni alloy, preferably in the presence of H_2 vapor (McCollom, 2013, 2016; McCollom et al., 2010). In natural hydrothermal systems, the synthesis of abiotic methane may rather be catalyzed by oxides present in mafic and ultramafic rocks (Foustoukos and Seyfried, 2004) during serpentinization. However, it is unclear whether natural fluids are saturated in vapor (Welhan, 1988, Charlou et al., 2010). Whether they offer a set of conditions allowing the rapid conversion of oxidized carbon to methane remains debated. Secondary fluid inclusions may be an alternative source of abiotic methane: worldwide oceanic peridotites and gabbros host vapor H_2- and CH_4-rich secondary fluid inclusions (Grozeva et al., 2020; Kelley and Früh-Green, 1999; Klein et al., 2019). Within the inclusions, a complex interplay of reactions between olivine, oxidized carbon and gaseous H_2 can lead to the synthesis of methane. As a result, inclusions contain up to 50 mole percent CH_4 (Grozeva et al., 2020; Kelley, 1996; Kelley and Früh-Green, 1999; Klein et al., 2019) and could be a large reservoir where abiotic methane formation occurs at temperatures below 400°C by reduction of trapped magmatic CO_2 (Klein et al., 2019, McDermott et al., 2015, Grozeva et al., 2020). Dissolution or fracturing of the olivine that hosts the inclusions could simply release abiotic methane in hot hydrothermal fluids, like at the Von Damm or Rainbow sites (Klein et al., 2019; McDermott et al., 2015). Regardless of the exact process of abiotic methane synthesis, it appears associated specifically with high temperature fluid-rock interaction in deep-sea hydrothermal systems.

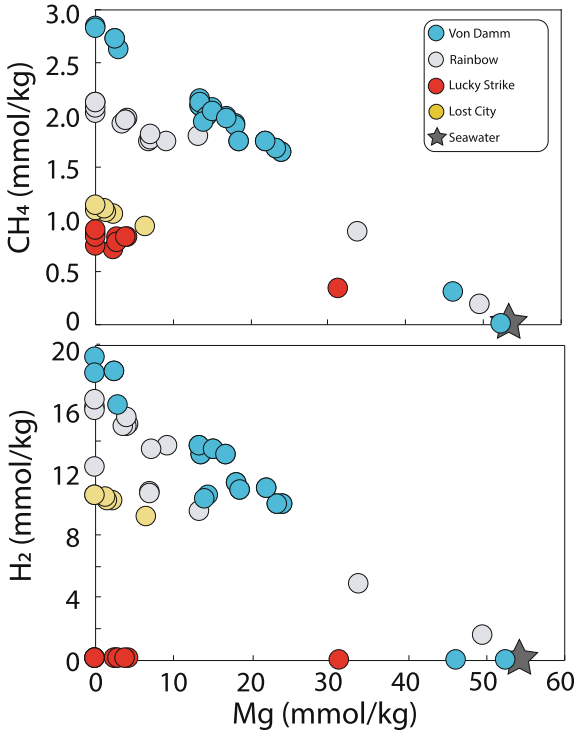

Fig. 1. Dissolved methane and hydrogen concentrations in hydrothermal fluids from the five locations studied here plotted against Mg concentrations. Data are from Reeves et al. (2014) and McDermott et al. (2015). With the exception of a sample from Vom Damm, *Ravelin*, all the samples studied here have Mg concentrations 5 mmol/kg (Data in Reeves et al., 2014, McDermott et al., 2015, and this study). *Ravelin*, however, shows a concentration of ~16 mmol/kg, together with a lower temperature than the local fluid endmember (Reeves et al., 2014). This one gas can be accounted for by seawater infiltration, abruptly lowering temperature venting.

In contrast to high temperature black-smoker vents, hot-springs venting at the Lost City hydrothermal field are characterized by considerably lower temperatures. However, Lost City fluids contain relatively high CH_4 and H_2 concentrations (Fig. 1), with isotopic and chemical signatures that are consistent with alkane abiogenesis (Lang et al., 2012; Proskurowski et al., 2008), similar to observations made in hotter fluids (McDermott et al., 2015). It is unclear whether fluids at Lost City record high-temperature events (Proskurowski et al., 2006) and subsequently underwent conductive cooling, or if low-temperature chemistry allowed the synthesis of abiotic alkanes. A complication is that the coldest vents at Lost City ($T < 60$ °C) host biofilms containing 106–109 cells per gram of carbonate, dominated by the Lost City Methanosarcinales (Brazelton et al., 2006; Kelley et al., 2005; Schrenk et al., 2004). These methanogens may contribute methane to the fluids at those vents (Bradley and Summons, 2010) and the contribution

The concentrations of the mass-18 isotopologues of methane, $^{13}CH_3D$ and $^{12}CH_2D_2$, can elucidate the origins and thermal histories of methane gases in hydrothermal fields. In $\Delta^{13}CH_3D$ versus $\Delta^{12}CH_2D_2$ space (Fig. 2), $^{13}CH_3D/^{12}CH_4$ and $^{12}CH_2D_2/^{12}CH_4$ ratios are reported relative to the stochastic distribution of isotopologues. In this diagram, methane in thermodynamic equilibrium with respect to isotopologue abundances falls on an equilibrium curve, where the relative abundances of rare isotopologues yield concordant temperatures (Fig. 2). When equilibrium signatures are observed, the assumption that methane isotopologue may constrain CH_4 thermometry (Stolper et al., 2014) may be valid (Young et al., 2017). In laboratory experiments, both biotic and abiotic methane exhibits disequilibrium deficits of $^{12}CH_2D_2$ at varying $\Delta^{13}CH_3D$ values (Giunta et al., 2019; Young et al., 2017). In the case of

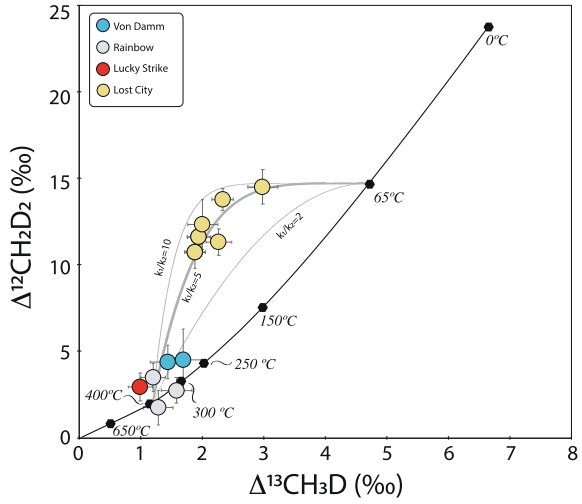

Fig. 2. Plot of $\Delta^{12}CH_2D_2$ vs. $\Delta^{13}CH_3D$ for methane samples from the hydrothermal vent systems that are part of this study. The curve representing thermodynamic equilibrium is shown for reference, along with corresponding temperatures. While Rainbow shows equilibrium signatures, Von Damm and Lucky Strike display marginally high $\Delta^{12}CH_2D_2$. The Lost City samples display considerable $\Delta^{12}CH_2D_2$ enrichments at a given $\Delta^{13}CH_3D$ value. Data and uncertainties are from Table 1. Re-equilibration trajectories are plotted using the equations in Section 5.3. Three scenarios are shown with three different ratios for the exchange rate constants for $\Delta^{12}CH_2D_2$ and $\Delta^{13}CH_3D$ (see text). Note that the endmember low temperature is picked at 65 °C for illustration. This corresponds to the approximate temperature of the fluid from *marker 2,* the coldest vent studied here. For the Beehive vent, a temperature of 96 °C would be required for the low-temperature endmember. Although not shown here for the sake of clarity, such an endmember temperature fits the Beehive data if $k1 \sim 5 \times k_2$.

microbial methane, kinetic controls result in anomalously low values for both $\Delta^{12}CH_2D_2$ and $\Delta^{13}CH_3D$ relative to formation-temperature estimates (Wang et al., 2015; Young et al., 2017). Such signatures were observed in sedimentary and lacustrine settings (Young et al., 2017; Giunta et al., 2019; Young 2019). Alternatively, partial reversibility of key enzymatic reactions during microbial methanogenesis (Stolper et al., 2015; Wang et al., 2015) and/or syntrophic microbial mediation (Ash et al., 2019; Giunta et al., 2019; Young et al., 2017; Young, 2019) could lead to biogenic methane characterized by equilibrium abundances of CH_4 isotopologues. Abiotic methane may exhibit peculiar signatures at high temperatures (Young et al., 2017); the few experimental data suggest $\Delta^{13}CH_3D$ may preserve CH_4 formation temperatures of abiotic methane, while $\Delta^{12}CH_2D_2$ can exhibit substantial depletions qualitatively similar to those produced by microbial methanogenesis. This pronounced abiotic disequilibrium in $\Delta^{12}CH_2D_2$ values is well illustrated by methane in ~25 °C fluids from the Kidd Creek mine, where CH_4 has been suggested to be abiotic in origin (Sherwood Lollar et al., 1993; Sherwood Lollar et al., 2006; Sherwood Lollar et al., 2002). There, $\Delta^{13}CH_3D$ values are broadly consistent with environmental temperatures in the mine and inferred temperatures of methane formation (Young et al., 2017; Sherwood Lollar et al., 2002) while remarkable $\Delta^{12}CH_2D_2$ depletions of up to ~25‰ relative to equilibrium are observed (Young et al., 2017). Although the $\Delta^{12}CH_2D_2$ formation temperatures are lost in this case, the disequilibrium isotopologue signature may be a diagnostic feature of abiotic methanogenesis (Young et al., 2017; Young, 2019). Based on these burgeoning but still unclear signatures of methane formation pathways, methane isotopologues may provide new constraints on the origin and/or the thermal history of CH_4 in hydrothermal vent settings.

Wang et al. (2018) published the first $\Delta^{13}CH_3D$ methane isotopologue data for deep-sea hydrothermal fields. At Rainbow, Lucky Strike, Von Damm, and Lost City, they measured a homogenous $\Delta^{13}CH_3D$ value of $\sim 1.6 \pm 0.3$‰. This value suggests a temperature of $^{13}CH_3D$ ordering of 310^{+53}_{-42} °C, indicating abiotic methane formed at high-temperatures contributes to all studied hydrothermal fluids, including the fluids at Lost City (Wang et al., 2018). Because the homogeneous $\Delta^{13}CH_3D$ is observed for fluids with varying exit temperatures (between 370 and 96 °C), it was suggested that $\Delta^{13}CH_3D$ ordering is preserved upon fluid cooling (Wang et al., 2018).

An original aspect of the clumped CH_4 systematics is that two doubly-substituted isotopologues can be measured independently (Young et al., 2016). Coupling these two species may help constrain the thermal history of methane. A current unknown is the relative behavior of $\Delta^{12}CH_2D_2$ compared to $\Delta^{13}CH_3D$ in hydrothermal fluids containing methane. It is unclear whether $\Delta^{12}CH_2D_2$ may provide new constraints on the origin of CH_4 in hot hydrothermal fluids. If so, we predict disequilibrium $\Delta^{12}CH_2D_2$ signatures will help track abiotic methane in natural samples, similar to signatures observed in the ~25 °C fluids at the Kidd Creek mine (Young et al., 2017). Alternatively, any $\Delta^{12}CH_2D_2$ abiotic signature may be erased at elevated temperatures, via re-ordering of the $^{12}CH_2D_2$ isotopologue. It is unclear whether $\Delta^{13}CH_3D$ would also be affected by re-ordering at all. In other words, potential re-ordering processes may cloud the meaning of the CH_4 systematics.

In the absence of experimental data on the behaviors of $\Delta^{12}CH_2D_2$ and $\Delta^{13}CH_3D$ in hot fluids, we present data on $\Delta^{13}CH_3D$ and $\Delta^{12}CH_2D_2$ measured in gases from deep-sea hydrothermal fluids sampled at Lucky Strike, Rainbow, Von Damm and Lost City. These fluids experienced variable extents of conductive cooling, allowing a test of whether $\Delta^{13}CH_3D$ and $\Delta^{12}CH_2D_2$ may be re-ordered in natural fluids. Ultimately, the data are used to examine how $\Delta^{13}CH_3D$ and $\Delta^{12}CH_2D_2$ may constrain the origin and/or the thermal evolution of methane in hydrothermal systems. Some of our samples are the same aliquots of gas analyzed for $\Delta^{13}CH_3D$ by laser spectroscopy by Wang et al. (2018), to which we add the first $\Delta^{12}CH_2D_2$ measurements. For Lost City, $\Delta^{13}CH_3D$ and $\Delta^{12}CH_2D_2$ measurements are reported for four new samples. Our samples from all of the sites span a large range of measured vent temperatures, from 65 to 370 °C. With these samples, we ascertain whether both mass-18 methane isotopologues record concordant temperatures of bond-ordering or if they record distinctive aspects of methane thermal history.

2. SAMPLES AND GEOLOGICAL CONTEXT

Rainbow is a hydrothermal field hosted in ultramafic rocks at 36°14′ N on the Mid-Atlantic ridge (MAR), at a water depth of 2300 meters (Charlou et al., 2002; Seyfried Jr. et al., 2011). At Rainbow, hydrothermal fluids have temperatures up to 370 °C and are the hottest fluids studied here. Hydrothermal fluids show chloride concentrations significantly higher than seawater, indicative of a brine-vapor phase separation occurring at depth at a minimum temperature of 380 °C (Charlou et al., 2002). The hydrothermal endmember contains ~2 mM CH_4 (Fig. 1) with a $\delta^{13}C$ of ~−15‰ (Charlou et al., 2002; Seyfried Jr. et al., 2011).

Lucky Strike is an unsedimented hydrothermal vent field hosted in basaltic rock, at 37°17′ N on the MAR, with fluid temperatures up to 324 °C (Charlou et al., 2000; Pester et al., 2012). Lucky Strike is a relatively shallow system with a seafloor depth of 1700 meters. There, the vent fluids have low silica, metal and rare earth content and are thought to reflect a rapid upflow of fluids to the surface with short water–rock reaction times (Charlou et al., 2000). Chloride concentration of hydrothermal fluids at Lucky Strike indicate the circulating seawater experienced brine-vapor phase separation at T > 360 °C, but at relatively low-pressure (Charlou et al., 2000). The methane concentration at Lucky Strike is ~1 mM (Fig. 1) with a $\delta^{13}C$ of ~−13‰ (Charlou et al., 2000; Pester et al., 2012).

The Von Damm site at 18°22′ N on the Mid-Cayman rise is hosted in ultramafic, gabbroic, and basaltic rocks, at 2350 meters below seafloor (Connelly et al., 2012). There, hydrothermal fluids emanate at temperatures as high as 226 °C (McDermott et al., 2015). Evidence that fluids experienced phase separation at Von Damm is inconclusive (McDermott et al., 2015). Methane concentration in the hydrothermal endmember is ~3 mM CH_4 (Fig. 1) with a $\delta^{13}C$ of ~−15‰ (McDermott et al., et al., 2015). For all high-temperature hydrothermal fields, δD data for CH_4 are scarce. To date, only Wang et al. (2018) published δD values for the studied sites, with all samples yielding values around −110 ± 15‰. These values are consistent with a D/H equilibrium between methane and water established during methane formation, at ~300 °C (Wang et al., 2018), based on the experimental data from Horibe and Craig (1995).

Lost City is located ~15 km west of the Mid-Atlantic Ridge in 1.5 my old lithosphere dominated by ultramafic rocks with minor mafic intrusions that have been exposed through detachment faulting. It is a serpentinite-hosted hydrothermal system, venting relatively cool (20–100 °C) fluids. In contrast with other systems studied here that vent acidic fluids, Lost City is the only field venting highly alkaline fluids with pH values >9 (Kelley et al., 2001, 2005). The lower temperatures at LCHF may be due to the location of the site, a few kilometers off the mid-Atlantic ridge axis and thus not directly above a localized heat source. The chlorinity of Lost City fluid is similar to seawater, suggesting no brine separation occurred beneath the Lost City hydrothermal field (Allen and Seyfried Jr., 2004). This is generally consistent with thermodynamic modelling suggesting maximum temperatures of 200 ± 50 °C (Foustoukos et al., 2008; Seyfried Jr. et al., 2015) although in the past mantle rocks in the Lost City basement experienced a higher-temperature alteration history (Früh-Green et al., 2018; Rouméjon et al., 2018). Maximum temperatures of 200 ± 50 °C for fluids currently circulating in the system appear to be lower than at the other sites, but the much cooler effusion temperatures of <100 °C nonetheless suggest that circulating fluids at Lost City underwent significant conductive cooling prior to venting.

Samples from Rainbow and Lucky Strike were collected by ROV Jason II during cruises to the Mid-Atlantic Ridge in 2008 (Pester et al., 2012; Reeves et al., 2014; Seyfried Jr. et al., 2011). Rainbow samples are from three vents: *Guillaume, Auberge*, and *CMSP_and_P* (all venting at 365 ± 10 °C). The sample from Lucky Strike is from the vent *Isabel* (venting at 292 °C). Samples from Von Damm were collected on the Mid-Cayman Rise in 2012 (McDermott et al., 2015). They are from two vents, *East Summit* (226 °C) and *Ravelin* (145 °C). Six Lost City samples were collected during the 2008 ROV Jason II cruise (J2-361-IGT5), the 2005 Lost City expedition (H06_GT_15/16) and the 2018 cruise to Lost City (J2-1107-GT9, J2-1111-Titan, J2-1110-GT18, J2-1110-Titan). They are from three vents: *Beehive* (~100 °C), *Marker C* (~85 °C), and *Marker 2* (~65 °C). Eight of our samples were previously analyzed by laser spectroscopy at MIT (Wang et al., 2018). Those were from Rainbow (n = 3), Von Damm (n = 3), Lucky Strike (n = 3) and Lost City (*Beehive* only, n = 1). The six remaining samples were not analyzed previously for either methane bulk isotope compositions nor for the rarer mass-18 methane isotopologues.

Due to near-zero concentrations of dissolved magnesium (Mg) in endmember hydrothermal vent fluids, measured Mg concentrations in sampled fluids can be used to estimate the extent of seawater entrainment during sampling or subsurface mixing. Concentrations of dissolved CH_4 concentrations plotted against dissolved Mg concentration for fluids from all sites studied are shown in Fig. 1 with data from the literature (Reeves et al., 2014; McDermott et al., 2015). Despite the considerable mixing shown in Fig. 1, we picked samples from Lucky Strike, Lost City, and Rainbow with low Mg concentration that can be considered to have minimal seawater contribution from sampling and thus more representative of the hydrothermal endmember. In contrast, based on Mg concentration reported in the literature, subseafloor seawater mixing before discharge occurred in some of the samples from Von Damm. One of our samples from a central vent (*Summit*) is devoid of seawater contamination and represents the local hydrothermal endmember, at 226 °C, while the other (*Ravelin*) shows evidence for subseafloor mixing with seawater that is reflected by a lower exit temperature of 145 °C (McDermott et al., 2015).

3. MEASUREMENT PROTOCOL

Methane was extracted from breakseals on a vacuum system at UCLA and purified by gas chromatography using procedures described previously by Young et al. (2017).

Between 40 and 120 micromoles of methane were available for each sample in our study (Table 1). Gases analyzed previously at MIT were subsequently trapped onto silica gel and sealed in quartz tubes for storage and transport to UCLA. At UCLA, the vacuum-line with a resting pressure of $3x10^{-5}$ mbar or lower was used to purify the samples. The gases were transferred from the breakseals into a silica gel-filled stainless-steel u-trap cooled with liquid nitrogen. Helium carrier gas was used to flush the sample to the gas chromatograph. Separation was accomplished with a 3 m long, 1/8 in. OD stainless steel column packed with 5 A molecular sieve, followed in series by a 2 m long 1/8 in. OD stainless steel column packed with HayeSep D porous polymer. Gas chromatograph peaks were detected with an in-line, passive thermal conductivity detector (TCD). Once methane collection was complete, methane was transferred to a glass vial filled with silica-gel at liquid nitrogen temperature and subsequently connected to the inlet of the Panorama mass spectrometer where it was warmed and expanded into the mass spectrometer.

Isotopologue measurements were made using the Panorama instrument, a Matsuda-type large radius high-resolution mass spectrometer at UCLA with a mass resolving power that allows the simultaneous measurement of ion currents for resolved $^{12}CH_4^+$, $^{13}CH_4^+$, $^{12}CH_3D^+$, $^{13}CH_3D^+$ and $^{12}CH_2D_2^+$ ion beams. The measured ratios of these ion currents yield values for both $\Delta^{13}CH_3D$ and $\Delta^{12}CH_2D_2$ as well as for bulk $^{13}C/^{12}C$ and D/H. The mass spectrometer is set to a mass resolving power equal to or greater than 40,000. Both low abundances of the mass-18 isotopologues, $^{13}CH_3D^+$, and $^{12}CH_2D_2^+$, require that measurements are made with an electron multiplier. Isotopologues of masses 16 and 17 are measured on Faraday collectors with amplifier resistors of 10^{11} Ω. The bulk carbon and hydrogen stable isotopic ratios are reported relative to the international standards V-PDB and V-SMOW, respectively, and expressed in permil units using the delta notation:

$$\delta^{13}C = [(^{13}C/^{12}C)_{sample}/(^{13}C/^{12}C)_{VPDB} - 1] \times 1000 \quad (1)$$

and

$$\delta D = [(D/H)_{sample}/(D/H)_{VSMOW} - 1] \times 1000 \quad (2)$$

Mass-18 isotopologue compositions are reported versus a stochastic distribution expressed in permil using the capital delta notation:

$$\Delta^{13}CH_3D = [(^{13}CH_3D/^{12}CH_4)_{sample}/(^{13}CH_3D/^{12}CH_4)_{stochastic} - 1] \times 1000 \quad (3)$$

and

$$\Delta^{12}CH_2D_2 = [(^{12}CH_2D_2/^{12}CH_4)_{sample}/(^{12}CH_2D_2/^{12}CH_4)_{stochastic} - 1] \times 1000 \quad (4)$$

The relationship between $\Delta^{13}CH_3D$ and $\Delta^{12}CH_2D_2$ and temperature has been predicted through *ab initio* calculations and can be represented by the following expressions (Young et al., 2017):

$$\Delta^{13}CH_3D\ (T) \approx 1000\ln(1 + 0.0355502/T - 433.038/T^2 + 1270210.0/T^3 - 5.94804 \times 10^8/T^4 + 1.196630 \times 10^{11}/T^5 - 9.07230 \times 10^{12}/T^6) \quad (5)$$

and

$$\Delta^{12}CH_2D_2\ (T) \approx 1000\ln(1 + 0.183798/T - 785.483/T^2 + 1056280.0/T^3 + 9.37307 \times 10^7/T^4 - 8.919480 \times 10^{10}/T^5 + 9.901730 \times 10^{12}/T^6) \quad (6)$$

where T is in Kelvin. These equations were verified using methane samples equilibrated over a range of temperatures in the UCLA laboratory (Young et al., 2017) and are consistent with gases equilibrated at low temperatures in other laboratories (Eldridge et al., 2019, Wang et al., 2019). Eqs. (5) and (6) show that when methane is formed at thermodynamic equilibrium, $\Delta^{13}CH_3D$ and $\Delta^{12}CH_2D_2$ are both positive, and must approach 0‰ at high temperatures (>1000 K).

Variable volume bellows for the sample and reference gases are adjusted after each measurement cycle of approximately 30 seconds so that ion current intensities are always balanced during the analyses. The mass spectrometry integration methods are described in Young et al. (2016). For standards and samples available in quantities >80 μmol, relative abundances of $^{13}CH_3D^+$ and $^{12}CH_2D_2^+$ are measured for up to 10 and 20 hours, respectively. In these cases, typical propagated internal errors for the calculation of $\Delta^{13}CH_3D$ and $\Delta^{12}CH_2D_2$ are generally ±0.1‰ and ±0.5‰, respectively. The external reproducibility is estimated based on repeated measurements of the thermogenic Utica shale gas, done with ~80 μmol of CH_4. Eight standards were measured over the course of this study (Supplementary Table 1), yielding average $\delta^{13}C$ and δD values of -25.81 ± 0.06‰ and -154.0 ± 0.1‰, and average $\Delta^{13}CH_3D$ and $\Delta^{12}CH_2D_2$ values of 2.8 ± 0.1‰ and 8.8 ± 0.8‰ (all 1 s.d.). In our study, often only 40–60 μmol of CH_4 were available (Table 1), and uncertainties are larger, reflecting less favorable counting statistics. The internal uncertainties range from 0.2‰ and 0.5‰ for $\Delta^{13}CH_3D$, and between 0.5‰ and 2.7‰ for $\Delta^{12}CH_2D_2$. Note that for all samples except two gases from Von Damm that yielded the smallest CH_4 quantities of the sample set, the internal uncertainties remained below 0.3‰ for $\Delta^{13}CH_3D$, and 1.0‰ for $\Delta^{12}CH_2D_2$.

4. RESULTS

Our bulk isotope ratios are in general agreement with previously-published CH_4 isotopic data for these localities (Charlou et al., 2002, Seyfried et al., 2011, 2015; Pester et al., 2012; McDermott et al., 2015; Wang et al., 2018, Proskurowski et al., 2008). In δD vs $\delta^{13}C$ space the samples plot in the ^{13}C- and D-enriched extremity of the abiotic methane field (Fig. 3) (Etiope and Sherwood Lollar, 2013). Comparison with the data of Wang et al. (2018) shows good agreement. Disagreement is found for one datum for sample J2-612-IGT2 from Von Damm where there is a discrepancy in δD between the two laboratories, with the UCLA value being lower by ~5‰. The UCLA datum for this sample also exhibit a low $\delta^{13}C$ value relative to the MIT value, consistent with a 1:10 $\delta^{13}C$ – δD fractionation that must have occurred between the moment it was measured at MIT and the moment it was measured at

Table 1
Methane isotope data for hydrothermal fluids. Bulk $^{13}C/^{12}C$ and D/H are reported alongside $\Delta^{13}CH_3D$ and $\Delta^{12}CH_2D_2$.

Site	Vent	Sample ID	CH_4 quantity (μmol)	Endmember temperature (C)	$\delta^{13}C$ PDB	δD SMOW	$\Delta^{13}CH_3D$	1 se	$\Delta^{12}CH_2D_2$	1 se
Rainbow	guillaume	J2-352-IGT4	38.8	361	−16.71	−98.06	1.6	0.3	2.7	0.8
	CMSP_and_P	J2-354-IGT3	51.3	365	−17.03	−98.49	1.2	0.2	3.5	0.8
	Auberge	J2-352-IGT3	46.8	370	−16.96	−98.07	1.3	0.2	1.7	1.0
Von Damm	Ravelin	J2-617-IGT6	45.0	226	−15.72	−107.26	1.4	0.3	4.4	1.0
	Summit	J2-612-IGT2	40.0	228	−16.50	−113.08	1.7	0.4	4.5	1.8
Lost City	Beehive	J2-361-IGT5	62.5	96	−10.80	−127.11	1.9	0.2	10.7	0.9
	Beehive	H06_GT_15/16	85.0	96	−10.84	−127.84	1.9	0.2	11.6	0.5
	Marker 2	j1107 GT	75.0	64	−9.62	−143.31	3.0	0.2	14.5	1.0
	Marker 2	J1111 titan	120.0	64	−7.58	−141.48	2.3	0.2	13.8	0.6
	Marker c	j1110 titan	90.0	81	−10.61	−129.70	2.3	0.2	11.3	0.8
	Marker c	j1110 GT	50.0	81	−10.97	−130.19	2.0	0.2	12.3	1.4
Lucky Strike	Isabel	J2-357-IGT5	47.5	292	−12.03	−100.72	1.0	0.2	2.9	0.7

Analytical uncertainties are below 0.1‰ (95% confidence intervals) for $\delta^{13}C$ and δD. Propagated uncertainties are listed for $\Delta^{13}CH_3D$ and $\Delta^{12}CH_2D_2$ in 1σ. They are variable from a sample to another, depending mostly on counting statistics. Hence the magnitude of the uncertainties for both $\Delta^{13}CH_3D$ and $\Delta^{12}CH_2D_2$ are a simple function of the processed CH_4 quantity (in μmol). Temperature data are extracted from the literature (McDermott et al., 2015; Reeves et al., 2014, but see also Pester et al., 2012; Charlou et al., 2010; Seyfried Jr. et al., 2011).

UCLA. We speculate that a fractionation could have occurred during incomplete sample freezing onto the silica gel in the quartz tube at MIT. Nonetheless, we determined a $\Delta^{13}CH_3D$ value from this gas that is indistinguishable from that reported by Wang et al. (2018), within uncertainties. This suggests that if a fractionation had occurred during the trapping of the sample at MIT, or during gas processing at UCLA, it was not sufficient to affect the apparent bond ordering.

Our methane isotopologues results (Table 1, Fig. 2) yield values of $\Delta^{13}CH_3D$ between 1.0 ± 0.2 and 3.0 ± 0.2‰, expanding the range of 1.0 ± 0.6 to 1.9 ± 0.3‰ reported by Wang et al. (2018) for deep-sea hydrothermal vent systems. No direct relationship is observed between the UCLA and MIT values, because of the narrow spread of the eight samples measured in both laboratories, and because of the relative uncertainties. For the first time, we report $\Delta^{12}CH_2D_2$ values for deep-sea hydrothermal methane, and we show the samples have values ranging from 1.7 ± 1.0‰ to 11.6 ± 0.5‰ (Table 1, Fig. 2). No $\Delta^{12}CH_2D_2$ values below zero are observed, in contrast with measurements of putative abiotic methane from the Kidd Creek mine (Young et al., 2017). Within analytical uncertainties, isotopologue abundances in samples from Rainbow are consistent with internal equilibrium with the ambient fluids (Fig. 2), with average $\Delta^{13}CH_3D$ and $\Delta^{12}CH_2D_2$ values of 1.4 ± 0.2‰ and 2.7 ± 0.9‰ ($n = 3$, both 1 s.d.), respectively. Samples from Lucky Strike and Von Damm show similar signatures, with $\Delta^{13}CH_3D$ data ranging from 1.0 ± 0.2‰ to 1.7 ± 0.4‰, and $\Delta^{12}CH_2D_2$ values that are slightly higher than values at Rainbow. At Von Damm, $\Delta^{12}CH_2D_2$ values are $+4.4 \pm 1.0$‰ and 4.5 ± 1.8‰ for *Ravelin* and *Summit* vents, respectively. In contrast, gases from Lost City are characterized by disequilibrium isotopologue signatures (Fig. 2). The Lost City samples exhibit $\Delta^{13}CH_3D$ values between 1.9 ± 0.2‰ and 3.0 ± 0.2‰ extending the range of values previously known for Lost City (Wang et al., 2018). $\Delta^{12}CH_2D_2$ values are between 10.7 ± 0.9‰ and 14.5 ± 1.0‰. The highest values are observed in *Marker 2*, the coolest vent, while *Beehive* and *Marker C* show consistent compositions. All methane from Lost City plots far above the equilibrium curve in $\Delta^{13}CH_3D$ vs. $\Delta^{12}CH_2D_2$ space. We find no relationships between the isotopologue signatures and host rock (whether hydrothermal fluids are hosted in basaltic versus ultramafic rocks), seafloor depth, or likely maximal pressures reached in the subsurface (Fig. 2). We argue below that the isotopologue signatures result from partial or near-complete re-equilibration of doubly-substituted isotopologues at environmental temperatures.

5. DISCUSSION

5.1. Equilibrium signatures for methane isotopologues

The methane isotopologue data for the hydrothermal systems studied here show signatures ranging from equilibrium to disequilibrium, from the hottest to the coldest fluids, respectively (Fig. 2). Samples from Rainbow have average $\Delta^{13}CH_3D$ and $\Delta^{12}CH_2D_2$ values that represent

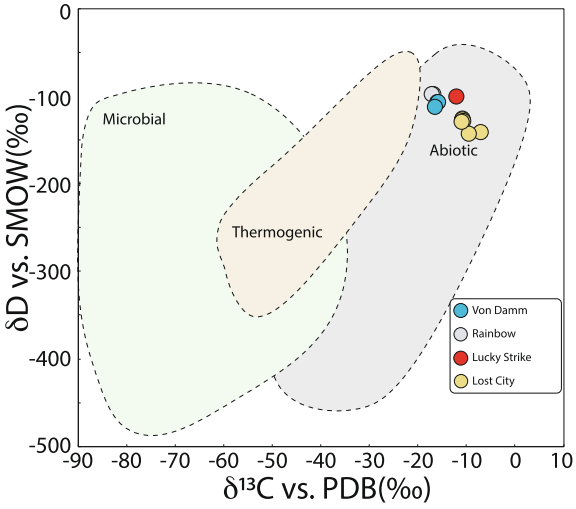

Fig. 3. δD and $\delta^{13}C$ values of methane samples in the "Schoell" plot (Schoell, 1988). Fields are suggested by those from Etiope and Sherwood Lollar (2013). As suggested in previous work (Wang et al., 2018; Proskurowski et al., 2008; Charlou et al., 2010; McDermott et al., 2015), methane in deep-sea hydrothermal fields is at the upper extremity of the abiotic field. Data and uncertainties are from Table 1.

thermodynamic equilibrium among the methane isotopologues. The $\Delta^{13}CH_3D$ values correspond to an apparent temperature of 343^{+41}_{-35} °C, similar to that derived previously (Wang et al., 2018). The temperature indicated by the $\Delta^{12}CH_2D_2$ values is 334^{+78}_{-53} °C, indistinguishable from that derived from the more abundant $^{13}CH_3D$ isotopologue, albeit less precise. This establishes that methane from Rainbow is in isotopic bond-ordering equilibrium.

Equilibrium could result from abiotic methane synthesis. This would be in contrast with deficits in $\Delta^{12}CH_2D_2$ where abiotic methanogenesis may have occurred at low temperatures at the Kidd Creek mine, where fluids carrying methane show measured temperatures of ~25 °C (Sherwood Lollar et al., 2002, Young et al., 2017). Equilibrium signatures in hot fluids could alternatively represent re-equilibration at high temperatures rather than being the result of the formation mechanism. Re-ordering is also suspected because disequilibrium $\Delta^{12}CH_2D_2$ signatures seem to be associated with abiotic CH_4 formation in laboratory experiments with durations from 12 to 30 days (Young et al., 2017). The few data for abiotic methane synthesized experimentally suggest $\Delta^{13}CH_3D$-based temperatures to be roughly consistent with experimental temperatures of abiotic CH_4 formation, while $\Delta^{12}CH_2D_2$ depletions of ~2–60‰ relative to equilibrium were observed between 75 and 500 °C. Only experiments where methane was synthesized at 600 °C during about 12 days yielded equilibrium for both $\Delta^{12}CH_2D_2$ and $\Delta^{13}CH_3D$ values (Young et al., 2017). We emphasize that it is unlikely that the experiments presented in Young et al. (2017) are an accurate representation of geochemical processes in deep-sea hydrothermal fields. It is interesting, however, that the two sets of experiments explored different formation mechanisms, the Fischer-Tropsch-type Sabatier reaction and silane hydration, and yielded broadly consistent results. In the silane experiments, $Si_5C_{12}H_{36}$ reacts with H_2O to produce SiO_2, CH_4 and H_2 (Foustoukos and Mysen, 2013) In the Sabatier processes, CO_2 is converted to CH_4 catalyzed with ruthenium at temperature <100 °C (Etiope and Ionescu, 2015). In both experiments, the large $\Delta^{12}CH_2D_2$ depletions may result from a quantum tunneling effect expressed during hydrogenation of methane precursors (Young et al., 2017). Alternatively, it may result from what is termed a "combinatorial effect" caused by mixing sources of hydrogen with markedly different D/H produced by classical kinetic and equilibrium partitioning of isotopes associated with the various hydrogenation steps during reduction of oxidized carbon (Cao et al., 2019; Young et al., 2017; Young, 2019). Hydrogen with wide ranging D/H ratios is sourced from different reversible and irreversible steps during methane formation, resulting in deficits in $\Delta^{12}CH_2D_2$ caused by mixing the various sources of hydrogen (Röckmann et al., 2016; Taenzer et al., 2020; Yeung, 2016). The two mechanistic interpretations described here both allow the preliminary experimental results from Young et al. (2017) to be extrapolated to natural settings, but further experimental work is needed.

In the context of the limited natural and experimental evidence, we tentatively suggest that equilibrium signatures at Rainbow (Fig. 2) might result from re-ordering rather than being inherited directly from abiotic methane synthesis. Secondary fluid-inclusions in gabbroic and ultramafic rocks likely contribute abiotic methane to hydrothermal fields (Kelley and Früh-Green, 1999; McDermott et al., 2015; McCollom, 2016; Klein et al., 2019). The inclusions may also provide conditions suitable for post-formation re-equilibration, since they contain metal oxides possibly contributing to catalysis (Klein et al., 2019; Grozeva et al., 2020) and would likely host methane over long periods of time. Alternatively, the concordant temperatures may reflect a rapid re-equilibration of all doubly-substituted isotopologues in the hot carrier fluid: at Rainbow, the $\Delta^{13}CH_3D$-based temperature of 343^{+41}_{-35} °C and the $\Delta^{12}CH_2D_2$ temperature of 334^{+78}_{-53} °C are both statistically indistinguishable from the temperature of the carrier fluid (360 ± 10 °C). Our data are therefore consistent with abiotic methane synthesis or re-equilibration in either the source fluid inclusions or in the carrier fluid at this site.

Methane from Lucky Strike and Von Damm show $\Delta^{13}CH_3D$ values similar to those at Rainbow, but display marginally higher $\Delta^{12}CH_2D_2$ values. Our one sample from Lucky Strike (from the *Isabel* vent) is virtually devoid of seawater contamination and is associated with a measured fluid temperature of 292 °C (Pester et al., 2012). The $\Delta^{13}CH_3D$ values of 1.0 ± 0.2‰ suggest a temperature of 430^{+60}_{-50} °C. The $\Delta^{12}CH_2D_2$ value of +2.9 ± 0.7‰ corresponds to an apparent temperature of 320^{+50}_{-39} °C. The latter estimate is within uncertainty of the measured fluid temperature (Fig. 4). At Von Damm, fluids are venting at a maximum temperature of 226 °C, but many of the fluids have experienced subseafloor mixing with cold seawater and

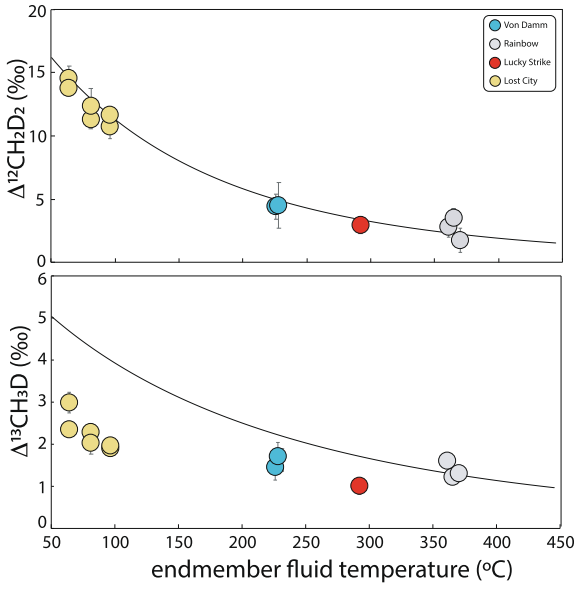

Fig. 4. Plot showing the relationship between the two mass-18 isotopologues of methane samples from the hydrothermal systems and the endmember temperatures of the fluid containing the methane. Note the correlation with fluid temperatures exhibited by $\Delta^{12}CH_2D_2$ but not $\Delta^{13}CH_3D$ values. Data and uncertainties are from Table 1.

are thus characterized by vent temperatures <226 °C (McDermott et al., 2015). The $\Delta^{13}CH_3D$ values are homogeneous and average 1.5 ± 0.2‰ which yields an apparent temperature of 325^{+40}_{-31} °C. The $\Delta^{12}CH_2D_2$ values are homogeneous as well but with an average of ~+4.5 ± 1.0‰, corresponding to a lower temperature of 247^{+43}_{-35} °C, similar to the measured hydrothermal maximum temperature of 226 °C (Fig. 4). We see no correlations between methane isotopologue data and the extent of subseafloor mixing with seawater (Table 1). The methane concentration of seawater is so low that arguably, seawater contamination does not add significant amounts of methane to the bulk vent fluid. We additionally conclude that both $\Delta^{13}CH_3D$ and $\Delta^{12}CH_2D_2$ values remain unaffected by the abrupt cooling associated with seawater infiltration.

Based on these results, we suggest that the methane isotopologue data at Rainbow, Lucky Strike and Von Damm are all consistent within 2σ with high-temperature methane formed at ~330 °C, as recorded by $\Delta^{13}CH_3D$. This thermometry is consistent with methane originating from secondary fluid inclusions, where thermodynamic modeling suggests it was synthesized over geological timescales at temperatures between 300 and 400 °C (Klein et al., 2019). Our results also imply re-ordering of the original $\Delta^{12}CH_2D_2$ values in the cooler carrier fluids. However, the $\Delta^{12}CH_2D_2$ re-ordering is about 2‰ and thus its detection is marginal given the measurement uncertainties of ~1‰. We show below that data obtained on the coldest site studied here, Lost City, are more dispositive with regard to the origin of discordance between $\Delta^{13}CH_3D$ and $\Delta^{12}CH_2D_2$ values.

5.2. Substantial $\Delta^{12}CH_2D_2$ re-equilibration or mixing in the cold Lost City fluids

Unlike at the other sites, at Lost City methane is carried to the seafloor by relatively cool fluids. The three vents examined, *Beehive* (~100 °C), *Marker C* (~85 °C), and *Marker 2* (~65 °C), show much lower temperatures than other vents studied here. The $\Delta^{13}CH_3D$ values are consistent with equilibration temperatures between 265^{+28}_{-24}°C and 158^{+16}_{-14}°C, far hotter than the measured fluid temperatures. The $\Delta^{12}CH_2D_2$ values yield temperature estimates of 101^{+9}_{-8} °C, 93^{+9}_{-8} °C and 69^{+4}_{-4} °C, showing a near-perfect match with the vent fluid temperatures (Fig. 4). The highest $\Delta^{13}CH_3D$ and $\Delta^{12}CH_2D_2$ values are observed in the coldest vent, *Marker 2*. These discordant isotopologue temperatures constitute marked disequilibrium (Fig. 2).

Before discussing the evidence of $\Delta^{12}CH_2D_2$ re-ordering at Lost City, we consider first whether the disequilibrium seen in the $\Delta^{13}CH_3D$ and $\Delta^{12}CH_2D_2$ data could be the result of mixing (e.g., Young et al., 2017). A relatively constant $CH_4/^4He$ ratio observed in Lost City vent fluids argues in favor of a unique abiotic source (Proskurowski et al., 2008; Lang et al., 2012). However, others have suggested a possible contribution from biotic sources (Bradley et al., 2009; Bradley and Summons, 2010); the coldest vents at Lost City (T < 60 °C) host biofilms dominated by the Lost City *Methanosarcinales* phylotype (Brazelton et al., 2006; Kelley et al., 2005; Schrenk et al., 2004). The methanogens may contribute significant microbial methane to the fluids at those vents (Bradley and Summons, 2010). In principle mixing between abiotic and microbial methane could account for the Lost City characteristic excesses in $\Delta^{12}CH_2D_2$. Our use of two mass-18 isotopologues affords the ability to identify mixing if it occurred at Lost City: mixing trajectories in $\Delta^{13}CH_3D$ versus $\Delta^{12}CH_2D_2$ space may trend above the equilibrium curve into positive $\Delta^{12}CH_2D_2$ deviations from equilibrium when endmembers are similar in $\delta^{13}C$ values but disparate in δD values. Multiple two-component mixing scenarios can satisfy mixing relationships in the isotopologue space. For example, in Fig. 5 we show a two-component mixing model between a gas equilibrated at 400 °C and a microbial gas with characteristic $\Delta^{12}CH_2D_2$ deficits. The high-T endmember $\delta^{13}C$ and δD values are taken to be similar to the values observed at Lucky Strike for illustration. Approximately 20 to 25% of a microbial gas mixed with high-temperature gas like that at the other vent sites can explain the methane isotopologue data at Lost City (Fig. 5, panel a). However, for the mixing loop to reach the compositions of the Lost City samples, unusually high $\delta^{13}C$ values of between –35‰ and −20‰ must be ascribed to the microbial methane component (Fig. 5, panel b). This is because the bulk isotopes and clumped isotopologue values, by design, do not vary independently. Such high $\delta^{13}C$ values would be considered unreasonable for microbial methane in most systems (Whiticar, 1999), but may be conceivable at Lost City, where biomarkers were observed with extraordinarily high $\delta^{13}C$ values (Bradley et al., 2009). This mixing scenario, however, fails to match the data trends where bulk isotope ratios are considered, including $\delta^{13}C$ vs. δD and $\Delta^{13}CH_3D$

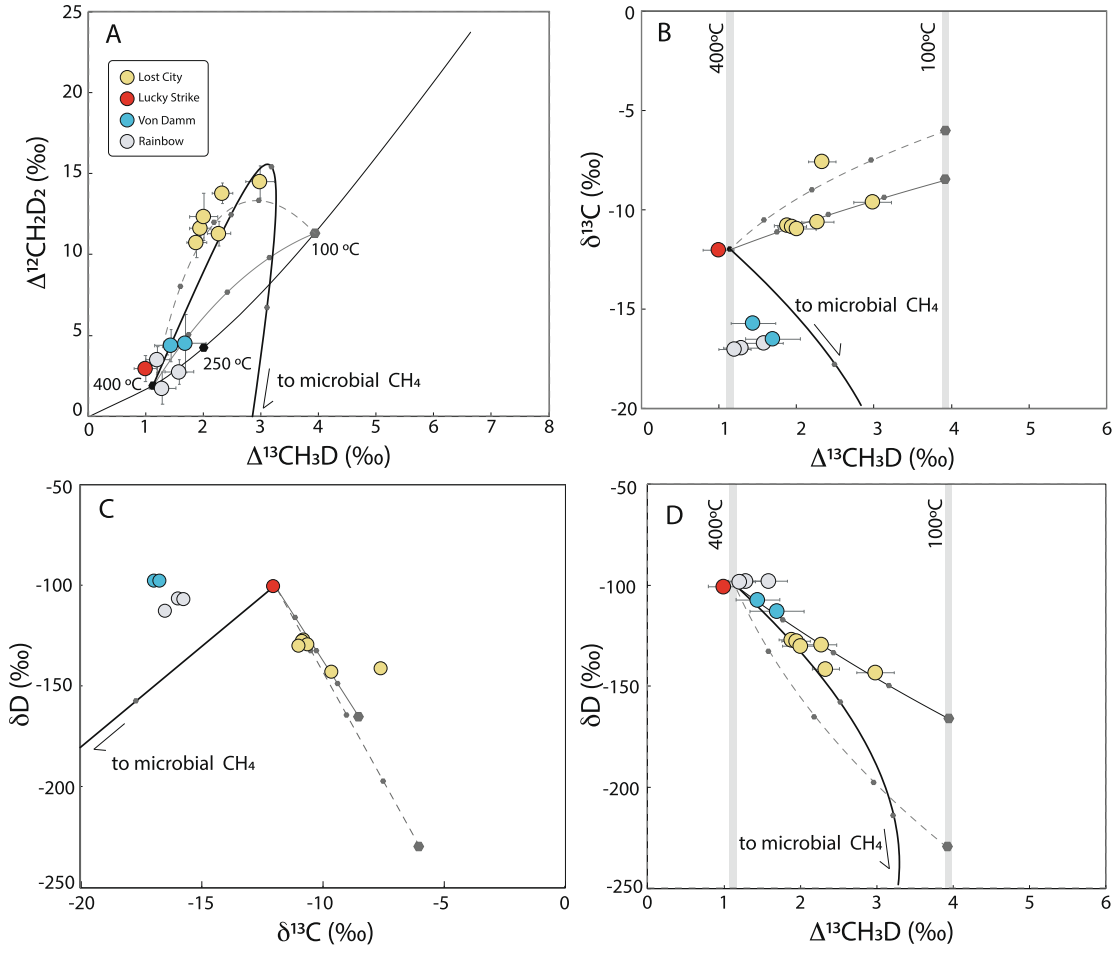

Fig. 5. Mixing scenarios for methane from Lost City, examined in 4 different CH4 isotopic spaces. Dots represent 25% increases in mixing increments. The bold curve is mixing between high-temperature gas and a microbial gas (see text) and shown by the bold plain curve. The dashed curve represents a two-component mixing between two equilibrated gases, at distinct temperatures, with endmember composition fit to account for the data in panel A and C. The plain thin curve is a two-component mixing between two equilibrated gases, at distinct temperatures, with endmember composition fit to account for the data in panel B, C and D. The panel A shows the two endmember possibilities that could fit the clumped isotopologue data, where $\Delta^{12}CH_2D_2$ is plotted vs. $\Delta^{13}CH_3D$. Panel B, C and D shows the various bulk-isotope trajectories of the model that is seemingly successful in panel A. We find no mixing scenario that accounts for all of the trends defined by the data.

vs. $\delta^{13}C$ (Fig. 5, panel b and c respectively). Conversely, when mixing is successful in panels comparing bulk isotopes and clumped isotopes (Fig. 5, panel b and d), it fails at accounting for the data in mass-18 isotopologue space (Fig. 5, panel a). For this reason, we conclude that mixing with a microbial methane component is not the main source of the anomalously high $\Delta^{12}CH_2D_2$ values at Lost City.

An alternative mixing scenario involves two gases both at isotopologue thermodynamic equilibrium at two disparate temperatures (Fig. 5). A ~50:50 mixing of two gases, one on the equilibrium curve at 400 °C, and the other on the equilibrium curve at any temperature <150 °C, could fit the Lost City isotopologue and bulk isotope data as long as the $\delta^{13}C$ and δD of the endmembers are restricted to a tight range of values. An example is shown in Fig. 5, with a gas taken at 100 °C for illustration (curve 2). The 100 °C gas at Lost City would have to have $\delta^{13}C$ values ≥−8‰, and corresponding δD values of −170‰ and lower. This is at the high- $\delta^{13}C$ and low-δD end of the empirically-defined abiotic field in Fig. 2 (Etiope and Sherwood Lollar, 2013; Whiticar, 1999). The high $\delta^{13}C$ would be consistent with the near-quantitative reduction of magmatic CO_2 (Horita and Berndt, 1999). The required δD value of −170‰ would indicate a methane-water D/H equilibrium established at low temperature compared to Rainbow, Lucky Strike, or Von Damm (Horibe and Craig, 1995), consistent with the bond-ordering inferences. However, again, this type of mixing relationship fails to account for the details of the data trend in panel b of Fig. 5. Where the mixing proportions needed in the isotopologue plot (Fig. 5, panel a) are roughly 50–50, they are about 80–20 in the bulk isotope space (Fig. 5 panel c), causing a mismatch in Fig. 5, panel b.

Mixing involving a microbial endmember seems to be ruled out, and mixing between gases equilibrated at high and low temperatures yields imperfect fits to the methane

isotopologue and bulk isotope data taken together. If mixing cannot satisfy the data in Fig. 5, we speculate that this is because $\Delta^{12}CH_2D_2$ was altered by re-ordering at the temperature of the ambient fluids in the vent system at shallow depths. The near-perfect match between $\Delta^{12}CH_2D_2$-based temperatures and fluid temperatures (Fig. 4) argues in favor of $\Delta^{12}CH_2D_2$ re-ordering. This conclusion is independent of the initial isotopologue composition of the abiotic methane, be it on the equilibrium curve or below the equilibrium curve, as observed with the limited experimental evidence (Young et al., 2017; see discussion above). We also suggest that the evidence for re-equilibration at Lost City (Fig. 4) allows re-equilibration to have occurred at high-temperatures sites like Rainbow (see Section 5.1). The mechanism of re-equilibration remains unclear. In the laboratory, methane isotopologues reorder only in the presence of a metal catalyst or alumina (Eldridge et al., 2019; Stolper et al., 2014; Wang et al., 2019; Young et al., 2017) when methane is in a gas phase, but no experiments exist for dissolved methane in water. At Lost City (and in all other deep-sea hydrothermal sites), methane is dissolved in water. Since $\Delta^{12}CH_2D_2$ is evidently re-ordered specifically at the exit temperature of the host fluids, the re-equilibration must have occurred in the cooling fluid upon ascent, perhaps facilitated by the metals that occur in underlying serpentinites at Lost City (Kelley et al., 2005, Früh-Green et al., 2018) or in metal deposits in chimneys observed at other sites (Von Damm, 1990). It is also possible that the re-equilibration of $\Delta^{12}CH_2D_2$ values is microbially mediated. The Archeal community at Lost City includes anaerobic methane-oxidizing Archaea, ANME-1 (Brazelton et al., 2006). Equilibration of $\Delta^{12}CH_2D_2$ values has been attributed to anaerobic oxidation of methane (AOM) at several localities, notably in gases from the Baltic Sea and the Western Ontario Basin (Young et al., 2017; Giunta et al., 2019; Ash et al., 2019). However, the evidence for equilibration by AOM has been circumstantial and yet to be demonstrated conclusively in the laboratory, and would not account for the equilibrated $\Delta^{12}CH_2D_2$ data at Rainbow, Von Damm and Lucky Strike, where temperatures are above 122 °C, often considered the upper limit for life (Takai et al., 2008).

In all cases, the data suggest that bond re-ordering is substantially slower for $\Delta^{13}CH_3D$, as if re-ordering was inhibited when the isotopologue includes ^{13}C rather than ^{12}C. The mechanism allowing one isotopologue, $^{12}CH_2D_2$, to be re-ordered to fluid temperature, while $^{13}CH_3D$ remains seemingly constant deserves experimental attention. The observation that $\Delta^{12}CH_2D_2$ is prone to re-equilibration at lower temperatures while $\Delta^{13}CH_3D$ is not suggests that the abundances of $^{13}CH_3D$ may represent a geochemical indicator that preserves information about temperatures associated with methane formation, even when the methane is transported at low temperatures prior to venting. The latter point is consistent with an earlier suggestion based on $\Delta^{13}CH_3D$ measurements alone (Wang et al., 2018), but it is verified and underscored by the contrasting behaviors of the two mass-18 isotopologues of methane at the vents studied here. The value of the $\Delta^{12}CH_2D_2$ values may lie with their sensitivity to subsequent environmental conditions.

A caveat to the basic picture described above arises from the observation of a ~1.5‰ $\Delta^{13}CH_3D$ variability at Lost City, when the *Beehive Marker C* and *Marker 2* vents are compared. To explain this in the context of just one high-temperature source of methane at Lost City (Lang et al., 2012), one must invoke partial re-ordering of $\Delta^{13}CH_3D$. The implication is that the cooling that resets $\Delta^{12}CH_2D_2$ values also partially re-equilibrates $\Delta^{13}CH_3D$ values. High-temperature methane formed at ~330 °C would exhibit $\Delta^{13}CH_3D$ values of ~1.5‰. At 85 °C, thermodynamic equilibrium drives $\Delta^{13}CH_3D$ to ~4‰. *Beehive*, *Marker C,* and *Marker 2* are vented at 96 °C, 81 °C and 64 °C, respectively, where the expectation of a $\Delta^{13}CH_3D$ trending towards ~4‰ because of partial re-equilibration is valid. One may speculate that cooling allowed partial reordering of $\Delta^{13}CH_3D$ to 1.9 ± 0.2‰ at *Beehive* and 2.3 ± 0.2‰ at *Marker C*. The ANME-1 identified at *Marker 2* (Brazelton et al., 2006) may be poorly suited to process methane in Lost City (Lang et al., 2018) but if any biological mediation of methane occurred, it might have affected $\Delta^{13}CH_3D$ at *Marker 2*, raising the values to 3.0 ± 0.2‰ there. The advantage of the hypothesis for partial $\Delta^{13}CH_3D$ re-equilibration at Lost City is that it explains why gases with higher $\Delta^{13}CH_3D$ are only observed in the coldest vents. It also removes the need for multiple methane pools, which is inconsistent with the broadly constant $CH_4/^4He$ ratio observed in the vents of Lost City (Proskurowski et al., 2008, Lang et al., 2012).

5.3. The relative vulnerability of $^{12}CH_2D_2$ to re-ordering

A process allowing $\Delta^{12}CH_2D_2$ to be equilibrated at fluid temperature during conductive cooling, while $\Delta^{13}CH_3D$ remains broadly constant, appears to account for natural data. This process calls for differences in re-equilibration rates. Here we explore this possibility with a simple kinetic model for exchange. Sophisticated models, where re-equilibration is driven by D/H exchange between methane and water, could be envisioned. In this context, water would be a reactive intermediate for re-ordering of methane isotopologues. At Lost City, this approach would be consistent with the overall lower D/H ratio for vented methane compared to other sites, suggesting some (but rather limited) D/H exchange occurred between methane and water during fluid cooling (Proskurowski et al., 2006; Reeves et al., 2012). As a first approximation, we explore the specific case of exchange of H and D between methane molecules. Our result based on molecular symmetry turns out to be the same if we use water as the exchange partner. In either case, the stretched bond permitting the fleeing of a protium or deuterium from a methane molecule is the reaction coordinate. We can describe the transition state formed by this stretching symbolically, in the case of CH_4, as CH_3-H. The relative magnitudes of rate constants for exchange reactions among isotopologues are dominated

by differences in symmetry numbers, as can be deduced from the analysis by Haghnegahdar et al. (2017). Indeed, both kinetic rate constants and equilibrium constants for the mass-18 isotopologues are controlled to first order by differences in symmetry numbers of the molecules. For example, the high-temperature limits for the equilibrium constants shown in Eqs. (5) and (6) are 1 and 3/8, respectively, both corresponding to the relevant ratios of reactant and product symmetry numbers.

Consider the reactions

$$^{12}CH_2D_2 + {}^{12}CH_4 \xrightarrow{k_1} {}^{12}CH_3D + {}^{12}CH_3D \quad (7)$$

and

$$^{13}CH_3D + {}^{12}CH_4 \xrightarrow{k_2} {}^{13}CH_4 + {}^{12}CH_3D \quad (8)$$

One may apply transition state theory and write the reaction in terms of the transition state for one molecule that will control the rate of the reaction, treating the deuterated reactant as rate limiting in a matrix of exchangeable CH_4 gas (or, as it turns out, H_2O). While the full equation that includes vibrational and rotational partition functions is necessary for capturing isotope ratios in detail at the per mil level of precision, the rate constant ratio can be well approximated for our purposes using the ratio of symmetry numbers for the transition states and the reactants where σ_i are the symmetry numbers. For this purpose, we use the known symmetry numbers for the reactants: $\sigma_{^{12}CH_4} = 12$, $\sigma_{^{13}CH_3D} = 3$, and $\sigma_{^{12}CH_2D_2} = 2$ and recall that the rotational partition functions are proportional to the inverse of the symmetry numbers. We estimate the likely symmetry numbers for the transition states CH_2D-D* and $^{13}CH_3$-D* based on previous work (Haghnegahdar et al., 2017). Stretching of the $^{12}CH_2D_2$ molecule to donate a D to $^{12}CH_4$ should result in a highly asymmetric transition state with $\sigma_{CH_2D-D^*} = 1$. The transition state for $^{13}CH_3D$ involves stretching the one ^{13}C-D bond, forming $^{13}CH_3$-D*, and preserving the symmetry of $^{13}CH_3D$, yielding $\sigma_{CH_3-D^*} = 3$. We therefore have for the rate constant ratio

$$\frac{k_{CH_2D_2}}{k_{^{13}CH_3D}} \sim \frac{\sigma_{CH_2D_2}\sigma_{CH_4}}{\sigma_{CH_2D-D^*}} \frac{\sigma_{^{13}CH_3-D^*}}{\sigma_{^{13}CH_3D}\sigma_{CH_4}} = \frac{2\times 12}{1}\frac{3}{3\times 12} = 2 \quad (9)$$

This result shows that the reaction involving the re-equilibration of $^{12}CH_2D_2$ can be expected to have a rate constant that is twice that for $^{13}CH_3D$. In practice, this means that during conductive cooling of a fluid, simple symmetry effects will lead $\Delta^{12}CH_2D_2$ to equilibrate twice as fast to environmental temperature than $\Delta^{13}CH_3D$. Because the symmetry number of the exchange partner ($^{12}CH_4$ as written) cancels in Eq. (9), substituting H_2O for $^{12}CH_4$, where $\sigma_{H_2O} = 2$, gives the same ratio of rate constants. We note, however, that the geometries associated with CH_4-H_2O exchange are highly uncertain (e.g., Van Mourik and Van Duijneveldt, 1995; Cappelletti et al., 2015; Richardson et al., 2016).

In order to apply these rate constants to the exchange process, we make use of rate equations for kinetic isotope exchange expressed in terms of fractional approaches to equilibrium (Criss et al., 1987) for the reactions in Eqs. (7) and (8), respectively:

$$\frac{[^{12}CH_2D_2]_t - [^{12}CH_2D_2]_{EQ}}{[^{12}CH_2D_2]_0 - [^{12}CH_2D_2]_{EQ}} = e^{-k_{CH_2D_2}t} \quad (10)$$

and

$$\frac{[^{13}CH_3D]_t - [^{13}CH_3D]_{EQ}}{[^{13}CH_2D]_0 - [^{13}CH_3D]_{EQ}} = e^{-k\,^{13}CH_3D^t} \quad (11)$$

where subscript t refers to time, subscript 0 refers to initial concentrations, and subscript EQ refers to the equilibrium concentrations for the isotopologues.

The re-equilibration mechanism with various rate constant ratios is plotted in Fig. 2, alongside the data. We explore whether the trajectory of a gas equilibrated at high temperatures undergoing cooling matches the Lost City observation. We take the low-temperature endpoint to be constrained by the measured temperature in the relevant Lost City vents, at 65 °C. Although the rate constant ratio of 2 resulting from Eq. (9) yields a trajectory in the right direction, it does not fully account for the data. We find that a rate constant ratio k_{CH2D2}/k_{13CH3D} of ~5 is required to explain the data (Fig. 2). Again, our data highlight the need for experimental work to explore whether these re-equilibration patterns are to be expected on a physicochemical basis. The simple theoretical framework explored here may offer a first order guide to how methane isotopologues behave during fluid cooling in natural settings.

6. CONCLUSION

We report $\Delta^{13}CH_3D$ and $\Delta^{12}CH_2D_2$ data in methane samples from deep-sea hydrothermal systems. We show that in the hottest fluids at the Rainbow site, concordant temperatures are recorded by the two mass-18 isotopologues. Thus, methane is in internal thermodynamic equilibrium. In the other sites, we observe variable $\Delta^{12}CH_2D_2$ at nearly constant $\Delta^{13}CH_3D$. The data exclude mixing with microbial gas; mixing produces imperfect fits to the bulk isotope ratios and isotopologue abundances. The variable $\Delta^{12}CH_2D_2$ values correlate surprisingly well with fluid temperatures and thus we suggest they record rapid $^{12}CH_2D_2$ re-equilibration in cooling hydrothermal fluids upon ascent. None of the isotopologue signatures resemble those obtained from experimental investigations of abiotic CH_4 synthesis in the laboratory, nor do they resemble the isotopologue signatures of abiotic methane formation in natural settings to date. The mechanism of re-equilibration in the case of these deep-sea hydrothermal fluids but not in the case of Kidd Creek cold fluids deserves experimental investigation. The discovery of resetting of $\Delta^{12}CH_2D_2$ values during transport affords the opportunity to use these values in concert with $\Delta^{13}CH_3D$ values to obtain a more complete picture of the thermal evolution of methane gases. This is because $\Delta^{12}CH_2D_2$ appears to be completely reset to fluid temperatures in a wide temperature range, between 360 and 65 °C. In contrast, $\Delta^{13}CH_3D$ shows limited evidence for re-ordering. We suggest that to first order, equilibration of $\Delta^{12}CH_2D_2$ should be faster than that for

$\Delta^{13}CH_3D$ by a factor of ~2, but further investigation of relative rates of reaction is warranted. Because the apparent $\Delta^{13}CH_3D$-based temperatures greatly exceed those amenable to microbial life in all sites, and because the isotopologue data rule out mixing with microbial gases, our data indicate that methane formation at all of the sites, including Lost City, is probably dominantly abiotic.

Declaration of Competing Interest

The authors declare that they have no known competing financial interests or personal relationships that could have appeared to influence the work reported in this paper.

ACKNOWLEDGEMENTS

We acknowledge support from the Deep Carbon Observatory Deep Energy grants G-2018-11346 and G-2017-9815 to EDY. We acknowledge Susan Lang for leading the 2018 Lost City cruise and for providing the temperature data funded by NSF-OCE-1536702 and a DCO-Deep Life sub-awards. We thank Tamara Baumberger for shipboard assistance with processing the gas samples. We thank Shuhei Ono and David Wang for sharing samples. We thank Orit Sivan and four anonymous reviewers for comments that improved the manuscript.

APPENDIX A. SUPPLEMENTARY MATERIAL

Supplementary data to this article can be found online at https://doi.org/10.1016/j.gca.2020.08.013.

REFERENCES

Allen D. E. and Seyfried, Jr., W. (2004) Serpentinization and heat generation: constraints from Lost City and Rainbow hydrothermal systems. *Geochim. Cosmochim. Acta* **68**, 1347–1354.

Ash J. L., Egger M., Treude T., Kohl I., Cragg B., Parkes R. J., Slomp C. P., Sherwood Lollar B. and Young E. D. (2019) Exchange catalysis during anaerobic methanotrophy revealed by 12CH2D2 and 13CH3D in methane. *Geochem. Perspect. Lett.* **10**, 26–30.

Berndt M. E., Allen D. E. and Seyfried W. E. (1996) Reduction of CO2 during serpentinization of olivine at 300 °C and 500 bar. *Geology* **24**, 351–354.

Bradley A. S., Hayes J. M. and Summons R. E. (2009) Extraordinary 13C enrichment of diether lipids at the Lost City Hydrothermal Field indicates a carbon-limited ecosystem. *Geochimica et Cosmochimica Acta* **73**(1), 102–118.

Bradley A. S. and Summons R. E. (2010) Multiple origins of methane at the lost City hydrothermal field. *Earth Planet. Sci. Lett.* **297**, 34–41.

Brazelton W. J., Schrenk M. O., Kelley D. S. and Baross J. A. (2006) Methane-and sulfur-metabolizing microbial communities dominate the Lost City hydrothermal field ecosystem. *Appl. Environ. Microbiol.* **72**, 6257–6270.

Cappelletti D., Bartocci A., Frati F., Roncaratti L. F., Belpassi L., Tarantelli F. and Pirani F. (2015) H2O–CH4 and H2S–CH4 complexes: a direct comparison through molecular beam experiments and ab initio calculations. *PCCP* **17**(45), 30613–30623.

Cao X., Bao H. and Peng Y. (2019) A kinetic model for isotopologue signatures of methane generated by biotic and abiotic CO2 methanation. *Geochim. Cosmochim. Acta* **249**, 59–75.

Charlou J., Donval J., Douville E., Jean-Baptiste P., Radford-Knoery J., Fouquet Y., Dapoigny A. and Stievenard M. (2000) Compared geochemical signatures and the evolution of Menez Gwen (37 50′ N) and Lucky Strike (37 17′ N) hydrothermal fluids, south of the Azores Triple Junction on the Mid-Atlantic Ridge. *Chem. Geol.* **171**, 49–75.

Charlou J. L., Donval J. P., Fouquet Y., Jean-Baptiste P. and Holm N. (2002) Geochemistry of high H2 and CH4 vent fluids issuing from ultramafic rocks at the Rainbow hydrothermal field (36°14′N, MAR). *Chem. Geol.* **191**, 345–359.

Charlou J. L., Donval J. P., Konn C., OndréAs H., Fouquet Y., Jean-Baptiste P. and Fourré E. (2010) High production and fluxes of H2 and CH4 and evidence of abiotic hydrocarbon synthesis by serpentinization in ultramafic-hosted hydrothermal systems on the Mid-Atlantic Ridge. *Divers. Hydrotherm. Syst. Slow Spread. Ocean Ridges* **188**, 265–296.

Connelly D. P., Copley J. T., Murton B. J., Stansfield K., Tyler P. A., German C. R., Van Dover C. L., Amon D., Furlong M. and Grindlay N. (2012) Hydrothermal vent fields and chemosynthetic biota on the world's deepest seafloor spreading centre. *Nat. Commun.* **3**, 1–9.

Criss R., Gregory R. and Taylor, Jr, H. (1987) Kinetic theory of oxygen isotopic exchange between minerals and water. *Geochim. Cosmochim. Acta* **51**, 1099–1108.

Eldridge D. L., Korol R., Lloyd M. K., Turner A. C., Webb M. A., Miller, III, T. F. and Stolper D. A. (2019) Comparison of experimental vs theoretical abundances of 13CH3D and 12CH2D2 for isotopically equilibrated systems from 1 to 500° C. *ACS Earth Space Chem.*.

Etiope G. and Ionescu A. (2015) Low-temperature catalytic CO 2 hydrogenation with geological quantities of ruthenium: a possible abiotic CH 4 source in chromitite-rich serpentinized rocks. *Geofluids* **15**, 438–452.

Etiope G. and Sherwood Lollar B. (2013) Abiotic methane on Earth. *Rev. Geophys.* **51**, 276–299.

Foustoukos D. I. and Mysen B. O. (2013) H/D methane isotopologues dissolved in magmatic fluids: Stable hydrogen isotope fractionations in the Earth's interior. *Am. Mineral.* **98**, 946–954.

Foustoukos D. I., Savov I. P. and Janecky D. R. (2008) Chemical and isotopic constraints on water/rock interactions at the Lost City hydrothermal field, 30°N Mid-Atlantic Ridge. *Geochim. Cosmochim. Acta* **72**, 5457–5474.

Foustoukos D. I. and Seyfried, Jr., W. E. (2004) Hydrocarbons in hydrothermal vent fluids: The role of chromium-bearing catalysts. *Science* **304**, 1002–1005.

Früh-Green G. L., Orcutt B. N., Rouméjon S., Lilley M. D., Morono Y., Cotterill C., Green S., Escartin J., John B. E. and McCaig A. M. (2018) Magmatism, serpentinization and life: Insights through drilling the Atlantis Massif (IODP Expedition 357). *Lithos* **323**, 137–155.

Giunta T., Young E. D., Warr O., Kohl I., Ash J. L., Martini A., Mundle S. O., Rumble D., Pérez-Rodríguez I. and Wasley M. (2019) Methane sources and sinks in continental sedimentary systems: New insights from paired clumped isotopologues 13CH3D and 12CH2D2. *Geochim. Cosmochim. Acta* **245**, 327–351.

Grozeva N. G., Klein F., Seewald J. S. and Sylva S. P. (2020) Chemical and isotopic analyses of hydrocarbon-bearing fluid inclusions in olivine-rich rocks. *Philos. Trans. R. Soc. A* **378**, 20180431.

Haghnegahdar M. A., Schauble E. A. and Young E. D. (2017) A model for 12CH2D2 and 13CH3D as complementary tracers for the budget of atmospheric CH4. *Global Biogeochem. Cycles* **31**, 1387–1407.

Holm N. G. and Charlou J. L. (2001) Initial indications of abiotic formation of hydrocarbons in the Rainbow ultramafic hydrothermal system, Mid-Atlantic Ridge. *Earth Planet. Sci. Lett.* **191**, 1–8.

Horibe Y. and Craig H. (1995) DH fractionation in the system methane-hydrogen-water. *Geochim. Cosmochim. Acta* **59**, 5209–5217.

Horita J. and Berndt M. E. (1999) Abiogenic methane formation and isotopic fractionation under hydrothermal conditions. *Science* **285**, 1055–1057.

Jones L. C., Rosenbauer R., Goldsmith J. I. and Oze C. (2010) Carbonate control of H2 and CH4 production in serpentinization systems at elevated P-Ts. *Geophys. Res. Lett.* **37**, L14306.

Kelley D. S. (1996) Methane-rich fluids in the oceanic crust. *J. Geophys. Res. Solid Earth* **101**, 2943–2962.

Kelley D. S. and Früh-Green G. L. (1999) Abiogenic methane in deep-seated mid-ocean ridge environments: Insights from stable isotope analyses. *J. Geophys. Res. Solid Earth* **104**, 10439–10460.

Kelley D. S., Karson J. A., Blackman D. K., FruÈh-Green G. L., Butterfield D. A., Lilley M. D., Olson E. J., Schrenk M. O., Roe K. K. and Lebon G. T. (2001) An off-axis hydrothermal vent field near the Mid-Atlantic Ridge at 30 N. *Nature* **412**, 145.

Kelley D. S., Karson J. A., Früh-Green G. L., Yoerger D. R., Shank T. M., Butterfield D. A., Hayes J. M., Schrenk M. O., Olson E. J. and Proskurowski G. (2005) A serpentinite-hosted ecosystem: the Lost City hydrothermal field. *Science* **307**, 1428–1434.

Klein F., Grozeva N. G. and Seewald J. S. (2019) Abiotic methane synthesis and serpentinization in olivine-hosted fluid inclusions. *Proc. Natl. Acad. Sci.*, 201907871.

Konn C., Charlou J.-L., Donval J.-P., Holm N., Dehairs F. and Bouillon S. (2009) Hydrocarbons and oxidized organic compounds in hydrothermal fluids from Rainbow and Lost City ultramafic-hosted vents. *Chem. Geol.* **258**, 299–314.

Lang S. Q., Butterfield D. A., Schulte M., Kelley D. S. and Lilley M. D. (2010) Elevated concentrations of formate, acetate and dissolved organic carbon found at the Lost City hydrothermal field. *Geochim. Cosmochim. Acta* **74**, 941–952.

Lang S. Q., Früh-Green G. L., Bernasconi S. M., Lilley M. D., Proskurowski G., Méhay S. and Butterfield D. A. (2012) Microbial utilization of abiogenic carbon and hydrogen in a serpentinite-hosted system. *Geochim. Cosmochim. Acta* **92**, 82–99.

Lang S. Q., Früh-Green G. L., Bernasconi S. M., Brazelton W. J., Schrenk M. O. and McGonigle J. M. (2018) Deeply-sourced formate fuels sulfate reducers but not methanogens at Lost City hydrothermal field. *Scientific reports* **8**(1), 1–10.

McCollom T. M. (2013) Laboratory simulations of abiotic hydrocarbon formation in Earth's deep subsurface. *Rev. Mineral. Geochem.* **75**, 467–494.

McCollom T. M. (2016) Abiotic methane formation during experimental serpentinization of olivine. *Proc. Natl. Acad. Sci. U. S. A.* **113**, 13965–13970.

McCollom T. M., Lollar B. S., Lacrampe-Couloume G. and Seewald J. S. (2010) The influence of carbon source on abiotic organic synthesis and carbon isotope fractionation under hydrothermal conditions. *Geochim. Cosmochim. Acta* **74**, 2717–2740.

McCollom T. M. and Seewald J. S. (2001) A reassessment of the potential for reduction of dissolved CO2 to hydrocarbons during serpentinization of olivine. *Geochim. Cosmochim. Acta* **65**, 3769–3778.

McCollom T. M. and Seewald J. S. (2007) Abiotic synthesis of organic compounds in deep-sea hydrothermal environments. *Chem. Rev.* **107**, 382–401.

McDermott J. M., Seewald J. S., German C. R. and Sylva S. P. (2015) Pathways for abiotic organic synthesis at submarine hydrothermal fields. *Proc. Natl. Acad. Sci.*.

Neubeck A., Duc N. T., Bastviken D., Crill P. and Holm N. G. (2011) Formation of H2 and CH4 by weathering of olivine at temperatures between 30 and 70 C. *Geochem. Trans.* **12**, 6.

Okland I., Huang S., Thorseth I. and Pedersen R. (2014) Formation of H2, CH4 and N-species during low-temperature experimental alteration of ultramafic rocks. *Chem. Geol.* **387**, 22–34.

Oze C., Jones L. C., Goldsmith J. I. and Rosenbauer R. J. (2012) Differentiating biotic from abiotic methane genesis in hydrothermally active planetary surfaces. *Proc. Natl. Acad. Sci.* **109**, 9750–9754.

Pester N. J., Reeves E. P., Rough M. E., Ding K., Seewald J. S. and Seyfried, Jr, W. E. (2012) Subseafloor phase equilibria in high-temperature hydrothermal fluids of the Lucky Strike Seamount (Mid-Atlantic Ridge, 37 17′ N). *Geochim. Cosmochim. Acta* **90**, 303–322.

Proskurowski G., Lilley M. D., Kelley D. S. and Olson E. J. (2006) Low temperature volatile production at the Lost City Hydrothermal Field, evidence from a hydrogen stable isotope geothermometer. *Chemical Geology* **229**(4), 331–343.

Proskurowski G., Lilley M. D., Seewald J. S., Früh-Green G. L., Olson E. J., Lupton J. E., Sylva S. P. and Kelley D. S. (2008) Abiogenic hydrocarbon production at Lost City hydrothermal field. *Science* **319**, 604–607.

Reeves E. P., McDermott J. M. and Seewald J. S. (2014) The origin of methanethiol in midocean ridge hydrothermal fluids. *Proc. Natl. Acad. Sci.* **111**, 5474–5479.

Reeves E. P., Seewald J. S. and Sylva S. P. (2012) Hydrogen isotope exchange between n-alkanes and water under hydrothermal conditions. *Geochim. Cosmochim. Acta* **77**, 582–599.

Richardson J. O., Pérez C., Lobsiger S., Reid A. A., Temelso B., Shields G. C. and Althorpe S. C. (2016) Concerted hydrogen-bond breaking by quantum tunneling in the water hexamer prism. *Science* **351**(6279), 1310–1313.

Röckmann T., Popa M. E., Krol M. and Hofmann M. (2016) Statistical clumped isotope signatures. *Sci. Rep.* **6**, 31947.

Rouméjon S., Früh-Green G. L., Orcutt B. N. and Party I. E. S. (2018) Alteration heterogeneities in peridotites exhumed on the southern wall of the atlantis massif (IODP expedition 357). *J. Petrol.* **59**, 1329–1358.

Schoell M. (1988) Multiple origins of methane in the Earth. *Chem. Geol.* **71**, 1–10.

Schrenk M. O., Kelley D. S., Bolton S. A. and Baross J. A. (2004) Low archaeal diversity linked to subseafloor geochemical processes at the Lost City Hydrothermal Field, Mid-Atlantic Ridge. *Environ. Microbiol.* **6**, 1086–1095.

Seewald J. S., Zolotov M. Y. and McCollom T. M. (2006) Experimental investigation of single carbon compounds under hydrothermal conditions. *Geochim. Cosmochim. Acta* **70**, 446–460.

Seyfried, Jr., W., Pester N. J., Ding K. and Rough M. (2011) Vent fluid chemistry of the Rainbow hydrothermal system (36 N, MAR): Phase equilibria and in situ pH controls on subseafloor alteration processes. *Geochim. Cosmochim. Acta* **75**, 1574–1593.

Seyfried, Jr., W., Pester N. J., Tutolo B. M. and Ding K. (2015) The Lost City hydrothermal system: Constraints imposed by vent fluid chemistry and reaction path models on subseafloor heat and mass transfer processes. *Geochim. Cosmochim. Acta* **163**, 59–79.

Sherwood Lollar B., Frape S., Weise S., Fritz P., Macko S. and Welhan J. (1993) Abiogenic methanogenesis in crystalline rocks. *Geochim. Cosmochim. Acta* **57**, 5087–5097.

Sherwood Lollar B., Lacrampe-Couloume G., Slater G., Ward J., Moser D., Gihring T., Lin L.-H. and Onstott T. (2006) Unravelling abiogenic and biogenic sources of methane in the Earth's deep subsurface. *Chem. Geol.* **226**, 328–339.

Sherwood Lollar B., Westgate T., Ward J., Slater G. and Lacrampe-Couloume G. (2002) Abiogenic formation of alkanes in the Earth's crust as a minor source for global hydrocarbon reservoirs. *Nature* **416**, 522.

Stolper D., Lawson M., Davis C., Ferreira A., Neto E. S., Ellis G., Lewan M., Martini A. M., Tang Y. and Schoell M. (2014) Formation temperatures of thermogenic and biogenic methane. *Science* **344**, 1500–1503.

Stolper D., Martini A., Clog M., Douglas P., Shusta S., Valentine D., Sessions A. and Eiler J. (2015) Distinguishing and understanding thermogenic and biogenic sources of methane using multiply substituted isotopologues. *Geochim. Cosmochim. Acta* **161**, 219–247.

Taenzer L., Labidi J., Masterson A. L., Feng X., Rumble, III, D., Young E. D. and Leavitt W. D. (2020) Low apparent Δ12CH2D2 in microbialgenic methane result from combinatorial isotope effects. *Geochim. Cosmochim. Acta*.

Takai K., Nakamura K., Toki T., Tsunogai U., Miyazaki M., Miyazaki J. and ... Horikoshi K. (2008) Cell proliferation at 122 C and isotopically heavy CH4 production by a hyperthermophilic methanogen under high-pressure cultivation. *Proceedings of the National Academy of Sciences* **105**(31), 10949–10954.

Von Damm K. L. (1990) Seafloor hydrothermal activity: black smoker chemistry and chimneys. *Annual Review of Earth and Planetary Sciences* **18**(1), 173–204.

Van Mourik T. and Van Duijneveldt F. B. (1995) Ab initio calculations on the CH. . .O hydrogen-bonded systems CH4-H2O, CH3NH2-H2O and CH3NH3+-H2O. *J. Mol. Struct. (Thoechem.)* **341**(1–3), 63–73.

Wang D. T., Gruen D. S., Lollar B. S., Hinrichs K.-U., Stewart L. C., Holden J. F., Hristov A. N., Pohlman J. W., Morrill P. L. and Könneke M. (2015) Nonequilibrium clumped isotope signals in microbial methane. *Science* **348**, 428–431.

Wang D. T., Reeves E. P., McDermott J. M., Seewald J. S. and Ono S. (2018) Clumped isotopologue constraints on the origin of methane at seafloor hot springs. *Geochim. Cosmochim. Acta* **223**, 141–158.

Wang D. T., Sattler A., Paccagnini M. and Chen F. G. (2019) Method for calibrating methane clumped isotope measurements via catalytic equilibration of methane isotopologues on γ-alumina. *Rapid Commun. Mass Spectromet.*.

Welhan J. A. (1988) Origins of methane in hydrothermal systems. *Chem. Geol.* **71**, 183–198.

Welhan J. A. and Craig H. (1979) Methane and hydrogen in East Pacific Rise hydrothermal fluids. *Geophys. Res. Lett.* **6**, 829–831.

Whiticar M. J. (1999) Carbon and hydrogen isotope systematics of bacterial formation and oxidation of methane. *Chem. Geol.* **161**, 291–314.

Yeung L. Y. (2016) Combinatorial effects on clumped isotopes and their significance in biogeochemistry. *Geochim. Cosmochim. Acta* **172**, 22–38.

Young E. D., Rumble, III, D., Freedman P. and Mills M. (2016) A large-radius high-mass-resolution multiple-collector isotope ratio mass spectrometer for analysis of rare isotopologues of O_2, N_2, CH_4 and other gases. *International Journal of Mass Spectrometry* **401**, 1–10.

Young E., Kohl I., Lollar B. S., Etiope G., Rumble, III, D., Li S., Haghnegahdar M., Schauble E., McCain K. and Foustoukos D. (2017) The relative abundances of resolved 12CH2D2 and 13CH3D and mechanisms controlling isotopic bond ordering in abiotic and biotic methane gases. *Geochim. Cosmochim. Acta* **203**, 235–264.

Young E. D. (2019) A two-dimensional perspective on CH4 isotope clumping: Distinguishing process from source. In *Deep Carbon: Past to Present* (eds. B. N. Orcutt, I. Daniel and R. Dasgupta). Cambridge University Press, Cambridge, pp. 388–414.

Associate editor: Orit Sivan